

The use of small angle neutron scattering with contrast matching and variable adsorbate partial pressures in the study of porosity in activated carbons

Z.Mileeva, D.K.Ross*, D.Wilkinson,

Materials and Physics Research Centre, Maxwell Building, University of Salford, Manchester, M5 4WT,
U.K.

S.M.King,

ISIS Facility, STFC, Rutherford Appleton Laboratory, Didcot, Oxon OX11 0QX, U.K.

T.A.Ryan, H.Sharrock.

Chemviron Carbon, Edgar House, Lockett Road, Ashton-in-Makerfield, Wigan, WN4 8DE, U.K.

(Received:)

Abstract

The porosity of a typical activated carbon is investigated with small angle neutron scattering (SANS), using the contrast matching technique, by changing the hydrogen/deuterium content of the absorbed liquid (toluene) to extract the carbon density at different scattering vector (Q) values and by measuring the p/p_0 dependence of the SANS, using fully deuterated toluene. The contrast matching data shows that the apparent density is Q -dependent, either because of pores opening near the carbon surface during the activation processor or changes in D-toluene density in nanoscale pores. For each p/p_0 value, evaluation of the Porod Invariant yields the fraction of empty pores. Hence, comparison with the adsorption isotherm shows that the fully dry powder undergoes densification when liquid is added. An algebraic function is developed to fit the SANS signal at each p/p_0 value hence yielding the effective

*Corresponding author: Tel/Fax +44 161 295 5881. E-mail d.k.ross@salford.ac.uk (D.K.Ross)

Kelvin radii of the liquid surfaces as a function of p/p_0 . These values, when compared with the Kelvin Equation, show that the resultant surface tension value is accurate for the larger pores but tends to increase for small (nanoscale) pores. The resultant pore size distribution is less model-dependent than for the traditional methods of analyzing the adsorption isotherms.

1. Introduction

The development of adequate methods of storing hydrogen on vehicles is one of the major barriers to the exploitation of hydrogen/fuel cell vehicle propulsion (see, for example Ross [1]). A promising route is through physisorption of H_2 on high surface area materials such as activated carbon. Such materials can achieve adequate gravimetric storage ($g H_2 / g$ material) at 80K but generally have a rather low volumetric storage capacity ($g H_2 / litre$ of bulk density as compared to the target given by – for instance - the US DOE¹). However, if hydrogen is stored in the activated carbon at high pressures, sufficient hydrogen is held in the open voids within the carbon to achieve attractive storage on the basis of combined pressurised gas and physisorbed H_2 . Moreover, this form of storage has the advantage of a low enthalpy of adsorption, meaning that target filling times can be reached with achievable cooling rates and also that, if an appropriate compacted form of carbon is used, the release of hydrogen in accident conditions will be much slower than for a simple high pressure storage system, hence decreasing the probability that the local H_2 concentration will exceed the lower explosive limit.

For this purpose, the development of a porous carbon, suitably compacted while retaining a high surface area – such that the hydrogen is adsorbed/desorbed at a controlled rate – is of great interest. A recent description of such carbons, particularly with reference to those derived from PEEK (poly-ether ether ketone), shows these to be some of the most promising systems for hydrogen storage [2]. It is the objective of the present paper to characterize the porosity of a typical activated carbon using SANS and hence to suggest ways of improving its performance for hydrogen adsorption.

¹ http://www1.eere.energy.gov/hydrogenandfuelcells/storage/current_technology.html

There are several well-established and commonly used techniques for characterizing porous media. These include gas sorption by volumetric or gravimetric methods, helium picnometry, mercury intrusion, SEM and other microscopies. Each of these techniques has its own limitations: gas adsorption techniques – whether volumetric or gravimetric (nitrogen BET methods and vapor adsorption isotherm measurements) – present difficulties in distinguishing between bulk and matrix densities; with helium picnometry, for nano-pores, there are uncertainties in the gas-matrix interactions; with mercury intrusion techniques, very high hydrostatic pressures are required to assess the micro-porosity of the sample and these can damage the internal porous structure. Finally, with SEM and related microscopies, only selected areas of the surface can be observed and such images do not provide quantitative information on the bulk or average porosity. It is therefore of interest to characterize the porosity of a particular activated carbon using small angle neutron scattering (SANS) and hence to suggest ways of improving its performance for hydrogen absorption. The technique provides direct and accurate measurement of the pore size distribution as a function of condensate partial pressure, combined with values for the matrix density [3-6]. In the present paper, we present the characterization of a typical activated carbon² by means of mercury and helium picnometry, BET and hydrogen adsorption (intelligent gravimetric analyser (IGA)³ measurements) and SANS using the contrast variation method with variable vapor partial pressure to investigate the process of pore filling. The method of partial pressure variation combined with SANS has been shown to yield useful information on the interconnectivity of porous systems. Thus, Li et al. [4] demonstrated that when contrast matched H₂O/D₂O is removed from porous Vycor by reducing the vapor partial pressure, the empty pores adopt the fractal geometry of a percolation network. This is because the necks between pores produced by etching the product of a spinodal decomposition process (as in Vycor) have a random variation and this system therefore generates a percolation network of empty pores, hence yielding a SANS signal with a Q^{-D} form. For adsorption of the liquid, on the other hand, the condensation takes place at random at narrow necks according to the Kelvin Equation, giving quite a different SANS signal for the adsorption isotherm. There have been few previous efforts to apply this complete

² Chemviron Carbon, SRD-2024/2

³ IGA002 from HIDEN Isochema, 231 Europa Boulevard, Gemini Business Park, Warrington, WA5 7TN U.K.

technique to porous carbons although Diduszko et al. [6] have compared pore size distributions in activated carbons as determined from SAXS with those derived from vapor adsorption curves. Further He et al. [7] have used the contrast matching method to study porosity in carbide-derived carbons while Mergia et al. [8] have similarly used this technique with D₂O to distinguish between open and closed pores in Zr and Ti-doped graphites while Mascotto et al. [9] have applied the SANS contrast match/partial pressure variation method to study the hierarchical pore geometry in a meso-porous silica. In the present carbons, as a result of the activation process applied - which presumably gives rise to progressively narrowing pore networks - no hysteresis loops are observed in the vapor adsorption isotherms, no percolation network is generated and hence the SANS simply gives a reversible measure of the unfilled pore volume as function of the partial pressure.

The organization of this paper is as follows. The sample preparation and characterization is described in Section 2. The SANS experiments are described in Section 3 while relevant aspects of the theory are described in Section 4. The analysis of the data is then described in Section 5 and the conclusions are given in Section 6.

2. Sample preparation and characterisation

The activated carbon employed² was in the form of extruded cylindrical pellets produced from powdered raw coal from several sources by steam activation. For a bulk specimen, the density has a unique value. For porous materials, however, there are three definitions of density: apparent or skeletal density (being the density of the sample excluding the accessible internal pore volume but including enclosed voids within the sample), bulk density (being the density of a certain volume of the sample including its open and closed porosity) and bulk tap density, observed in terms of space filling after the powder has been tapped. For present purposes, the most relevant value is the skeletal density.

2.1 IGA measurements

In order to characterize the activated carbon further, an Intelligent Gravimetric Analyser (IGA)³ [10] was employed to measure values of the specific surface area, the skeletal density, the pore size distribution and the hydrogen

sorption capacities at both ambient and liquid nitrogen temperatures. An activated carbon sample of about 100 mg was loaded into the IGA and was out-gassed under vacuum using a series of temperature steps in the sequence: 200°C, 300°C, 400°C and 500°C. The resulting weight change profile was recorded. It was found that the mass only achieved an asymptotic value after a period of heating at 500°C. The IGA was then used to measure the BET surface area of this out-gassed sample by measuring the mass gain as a function of the pressure of dry nitrogen at 80K. The standard BET equation was used to analyze the data from both adsorption and desorption isotherms. The BET surface area, thus determined, was 1188 m²/g. The BET surface area was also measured by the non-standard method of applying the BET equation to the toluene sorption isotherm as measured at room temperature. The value obtained, of 1190 m²/g, is close to that determined with nitrogen, suggesting that toluene molecules effectively access micro-pores. The total pore volumes determined by nitrogen and toluene adsorption with IGA are 0.727 cc/g (measured at 0.73 p/p₀) and 0.716 cc/g (measured at 0.72 p/p₀) respectively. The pore size distribution (PSD) of the carbon was derived from the nitrogen adsorption data using the De-Boer [11], the Halsey [12] and the Dubinin-Astakhov [13] PSD analyses. The De-Boer analysis (implying a peak in the pore size probability distribution at 10.5 Å) and the Halsey analysis (implying peak at 10.3 Å) are both model-dependent and are based on the relationship between the nitrogen pressure, the thickness of an adsorbed layer on the pore wall and a core radius, whereas the

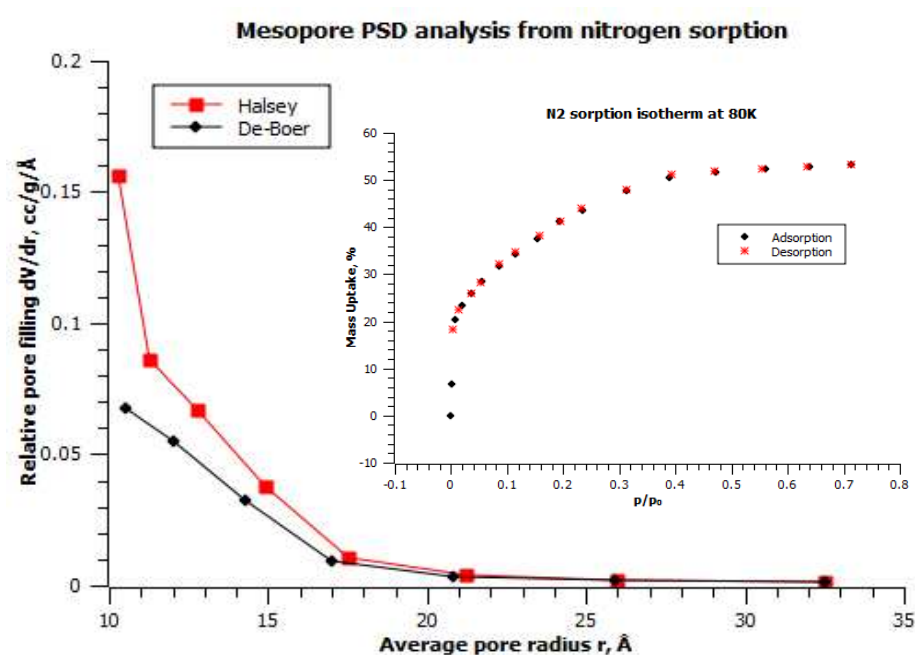


Fig. 1. Pore size distribution according to De-Boer and Halsey models from nitrogen sorption. Inset: Nitrogen sorption isotherm at 80K.

Dubinin-Astakhov analysis (which yields a peak in the PSD at 9.4 Å) is a partly empirical approach. Nevertheless, the Pore Size Distributions obtained from these three approaches show very similar behavior, indicating a peak in the distribution at around 10 Å (Figs.1). Because of the assumptions involved, the first two models only work down to pore sizes of 10 Å. The Pore Size Distribution

was also obtained from the toluene adsorption isotherm using the De-Boer, the Halsey (Fig. 2) and the Dubinin-Astakhov method (yielding a peak at 7.8 Å) analyses.

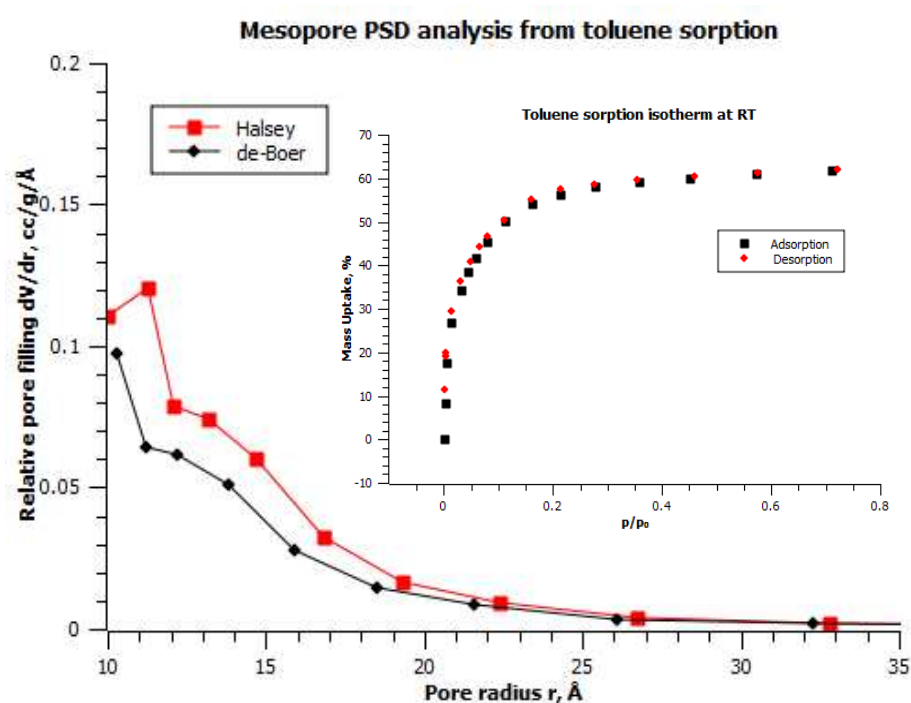


Fig. 2. Pore size distribution according to De-Boer and Halsey models from toluene sorption. Inset: Toluene sorption isotherm at RT.

Hydrogen was then introduced into the IGA to measure the amount of H₂ adsorption as a function of pressure at both 77K and room temperature. For this particular activated carbon, it was found that, at 15 bar hydrogen pressure and 77K, 2.6% mass uptake was observed while, at ambient temperatures, at the same pressure, 0.1% by mass was adsorbed. Both isotherms were fully reversible. The time dependence of the hydrogen

adsorption was also obtained from the IGA measurements at 80K. These vary with hydrogen pressure but are of the order of 40 s. The density of the sample was also measured at ISIS, RAL, using a Quantachrome micro-pycnometer. The density determined by this technique was 2.035 g/cc.

Small Angle Neutron Scattering measurements

The SANS measurements were performed using the LOQ instrument⁴ at the ISIS Pulsed Neutron Source, Rutherford Appleton Laboratory. LOQ is a fixed-geometry “white beam” time-of-flight instrument that utilizes neutrons with wavelengths, λ , between 0.2 and 1 nm. Data are simultaneously recorded on two, 2-D, position-sensitive neutron detectors, overlapping in Q space, to provide a simultaneous Q range of 0.006–1.6 Å⁻¹. Here the wave vector transfer is $Q = (4\pi/\lambda) \sin \theta$ where θ is the scattering angle.

⁴ <http://www.isis.stfc.ac.uk/instruments/loq/>

3.1 Contrast matching experiments

A sample of the activated carbon was first crushed into a fine powder and then outgassed as above. The contrast matching experiments were performed using mixtures of normal and fully deuterated toluene of accurately controlled compositions. Toluene was chosen because it gave close to the maximum possible neutron scattering density in its deuterated form (the nearest scattering length density to that of carbon) and because toluene is known to fully wet carbons [3]. In order to record directly comparable SANS data sets, equal amounts of carbon were loaded into standard quartz cuvettes (Hellma⁵). The various isotopic mixtures of toluene were then added to the carbon and the sealed cuvettes were left in an ultrasonic bath contained in a glove bag under an argon flow to ensure that all the pores were filled/wetted. Each sample was 2 mm thick and had a total silica wall thickness (front + back) of 2mm.

3.2 Variable partial pressure experiments

For the second experiment, where the partial pressure of deuterated toluene was to be set to various values between vacuum and just below the saturated vapor pressure of toluene, a special sample cell was designed. This Al alloy cell consisted of 2 half-cells and a holder (designed to be mounted on the sample table). The two halves were sealed together using indium wire. Rod heaters to control the sample temperature were inserted into holes drilled in the outer ring. The cell was connected to a pressure transducer and an isolation valve and hence to a source of the fully deuterated toluene vapor by means of a stainless steel tube (Fig. 3). Following the out-gassing procedure described above - using a separate sample tube - the carbon was loaded into the cell under argon, the two halves of the cell were sealed together and the assembly was evacuated. Extra care was taken to ensure that no impurity gas was admitted to the cell. The cell was then mounted in the beam, the valve to the D-toluene source was opened and the partial pressure was allowed to reach the first point to be measured. Deuterated toluene sorption and desorption cycles were performed at a series of steps in partial pressure, with the cell held at 46°C. The rest of the system

⁵ Hellma Analytics, quartz cell manufacturer.

(tubing, pressure transducer, toluene source) was maintained at a temperature just above the sample temperature and this was constantly monitored during the experiment to avoid condensation anywhere other than in the sample.

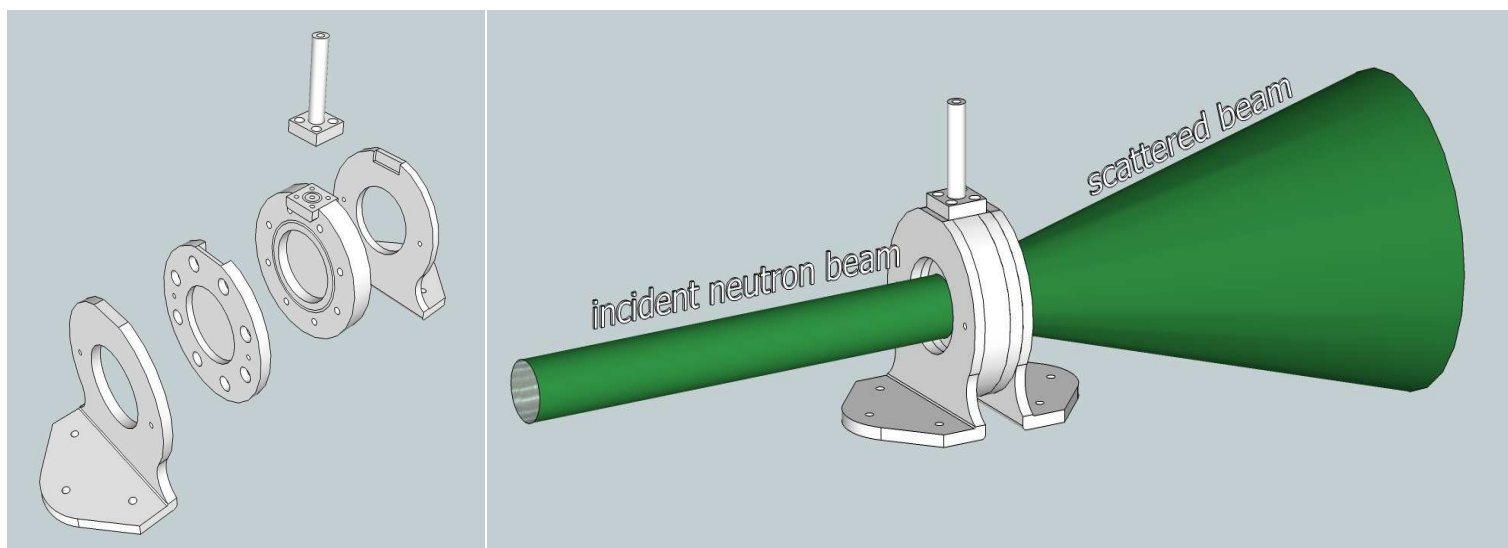


Fig. 3. Exploded view of the cell and sample holder used for the variable partial pressure experiments and their position in the neutron beam line.

After the experiment, a mass spectrometer analysis was performed to confirm that only deuterated toluene was present.

3.3 Data treatment

To gather data of sufficiently high statistical precision, it was found necessary to measure each new contrast-match sample or p/p_0 setting for around 70 minutes while collecting 30 μ Amps of incident beam current, depending on the contrast conditions (see Section 4.2). Each different partial pressure sample was left for about an hour for the pressure to equilibrate before taking the actual measurements. The raw scattering data sets were then normalised to the incident wavelength distribution and corrected for the detector efficiencies, the measured transmission, and the background scattering (as measured using an empty quartz cuvette or Al cell), before being converted to scattering cross-section values ($\partial\Sigma/\partial\Omega$ versus Q) using the instrument-specific software [14]. These data were placed on an absolute scale (cm^{-1}) by comparison to the scattering from a standard sample (a solid blend of hydrogenous and per-deuterated polystyrene), measured with the same instrument geometry, in accordance with established procedures

[15]. The accuracy of this inter-normalization is well established and is particularly important for the present experiment.

4. Theory of Small Angle Neutron Scattering: fractals, contrast matching and variation of the SANS signal with partial pressure

4.1 Small Angle Neutron Scattering from fractals

The SANS scattering intensity (or the number of neutrons of a given wavelength per unit time scattered by a sample into a detector subtending a solid angle $\Delta\Omega$ at a wave vector transfer, Q) is given by⁶ [16]:

$$I(Q) = I_0(\lambda)\Delta\Omega\eta(\lambda)TV \frac{d\Sigma}{d\Omega}(Q) \quad (1)$$

Here, $I_0(\lambda)$ is the incident neutron flux/unit wavelength, $\eta(\lambda)$ is the detector efficiency, T is the sample transmission, V is the sample volume and $d\Sigma/d\Omega(Q)$ is the differential scattering cross section which is the Fourier Transform of the neutron scattering length density-density correlation function of the pores – assuming that the matrix has a fixed density. The crucial term is the differential scattering cross section which, for pores in carbon, can be written in terms of the neutron scattering length density of the carbon, ρ_c and of the scattering density in the pore, ρ_p :

$$\frac{d\Sigma}{d\Omega}(Q) = N_p V_p^2 (1 - N_p V_p)(\rho_c - \rho_p)^2 S(Q)F^2(Q) + B_{inc} \quad (2)$$

Here, N_p is the number of pores/unit volume, V_p is the volume of the pore, $S(Q)$ is the structure factor for the separation of the pore centers and $F^2(Q)$ is the form factor for the pores. B_{inc} is the flat (Q -independent) background which will be dominated by any incoherent scattering if present but will also contain any instrument background not perfectly subtracted during data analysis. Strictly speaking, V_p should be $\langle V_p \rangle$ and $F^2(Q)$ should be $\langle |F(Q)|^2 \rangle$ i.e. both are averaged over the pore size distribution. Here, we have assumed that the inter-pore structure factor, $S(Q)$,

⁶ S.M. King: http://www.small-angle.ac.uk/dms/small-angle/Intro_to_SANS_Web.pdf

is not correlated to the pore size and that the pores have no preferred orientation. The assumption underlying this expression is that Babinet's Principle is applicable (i.e. we can reverse ρ_c and ρ_p without affecting the scattering signal). As the density-density correlation function in space is a convolution of the pore size with the inter-pore correlation, after Fourier Transformation, the resulting functions of Q appear as products. Writing this out formally, the form factor is:

$$F^2(Q) = \left| \int_{\text{pore_volume}} \frac{e^{i\mathbf{Q}\mathbf{r}}}{\langle v_p \rangle} d\mathbf{r} \right|^2 \quad (3)$$

Similarly the structure factor is:

$$S(Q) = \left\langle \frac{1}{N} \sum_{i,j} e^{-i\mathbf{Q}(\mathbf{r}_i - \mathbf{r}_j)} \right\rangle \quad (4)$$

Here, again, the averaging is over all pores present where \mathbf{r}_i and \mathbf{r}_j represent the centres of the i^{th} and j^{th} pores respectively. It should be noted that if all the pores are filled with liquid having a scattering length density, ρ_{liq} , this could be substituted for ρ_p that would normally be zero. Clearly, therefore, the SANS will disappear completely if $\rho_{\text{liq}} = \rho_c$.

It should be noted that this formulation of the SANS signal is directly applicable to what might be described as the current bun type of porosity where, in particular, the pore surfaces are smooth. The separation into $F^2(Q)$ and $S(Q)$ is much less obviously appropriate to interconnected porosity with rough surfaces.

It is often found in porous materials such as carbons that $d\Sigma/d\Omega(Q)$ can be represented by a power law with a non-integer negative exponent This indicates the presence of a pore fractal [17-19] and allows us to define the form of $S(Q)$. Fractals are defined as materials in which the geometric structure is independent of the length scale on which it is observed. This is strictly true for geometric fractals such as those investigated by Mandelbrot [20]. More commonly in Nature, as in the present case, the features are actually random, being only self-similar when viewed

on different length scales, i.e. the material is produced from e.g. a vegetable source which is typically fractal and, after pyrolysis, it retains the fractal geometry of the original material. Three classes of fractal can be identified: (1) volume fractals – where the average density of a material decreases in a power law fashion as one moves out radially from an origin chosen to be in the solid phase. Such material is said to have a volume fractal dimension of D_m (<3 in a 3-D space); (2) pore fractals, where the distribution of pore volume decreases in a similar way with increasing distance from a pore centre. These would thus have a pore fractal dimension of D_p (<3 in 3D); (3) surface fractal – where the measured surface area increases in a power law fashion when measured using a decreasing tile size. Here the non-integer dimension is D_s where $2 < D_s < 3$. In general, the fractal behavior will only exist over a limited length range (but should be over at least an order of magnitude in length), between the lower and upper fractal limits, L_{min} and L_{max} respectively. When, for these three types of fractal, the density-density correlations are converted to the differential scattering cross section form, we find that the scattering will in general vary as [21]:

$$S(Q) \sim Q^{D_s - 2(D_m + D_p) + 6} \quad (5)$$

For a surface fractal, we take $D_m = D_p = 3$ so that $I(Q) \sim Q^{D_s - 6}$ as first derived by Bale and Schmidt [5]. Here, in general, the scattering will vary with powers of Q between -3 and -4. For a volume fractal, we take $D_s = D_m$ and $D_p = 3$ so that $S(Q)$ varies as Q^{-D_m} while for a pore fractal, we similarly get $S(Q) \sim Q^{-D_p}$. The upper and lower fractal limits can also be introduced into the analysis. Freltoft et al. [22], for instance, obtained an algebraic expression using an exponential expression to cut off the upper fractal limit and a step function for the lower limit - corresponding to $2r_0$ where r_0 can be taken to be the pore radius.

In order to model the full scattering function, we also need to model the form factor for the pores, $\langle F^2(Q) \rangle$. The most reasonable form factor for pores produced by the activation process would be a Gaussian, and from this, we derive the Guinier form of $F^2(Q)$ namely:

$$F^2(Q) = e^{-\frac{Q^2 r_0^2}{5}} \quad (6)$$

where r_0 is the radius of a sphere with the same radius of gyration. The proper calculation for a spherical pore shows considerable structure at high Q but if a range of pore diameters are included, this structure is averaged out and in general we can obtain a value of $\langle r_0^2 \rangle$ from a fit to the Guinier Equation [22, 23]. For many systems, we might want to consider a distribution of pore sizes – a poly-disperse system. For instance, a power law distribution of pore radii gives a power law distribution of scattering in Q space – an alternative to the fractal model (see section 5.2). Thus, in practice for more complex porosity, the distinction between $F^2(Q)$ and $S(Q)$ becomes somewhat arbitrary.

4.2 Contrast matching and vapor pressure variation

“Contrast matching” in SANS involves a determination of the scattering length density of the matrix by varying the scattering length density of the liquid introduced into the pores and hence determining how the magnitude of the contrast term, $(\rho_c - \rho_{\text{liq}})^2$, varies with ρ_{liq} - in particular, at which value of ρ_{liq} this term goes to zero. The particular advantage of this technique with H/D toluene is due to the fact that the contrast can be varied over a large range in scattering density because of the large difference in scattering lengths between hydrogen (negative) and deuterium (positive). We can thus change the scattering length density of the pore-filling medium so that different features of the sample can be illuminated. We have chosen to use toluene for the present experiment because it is known to wet the surface of carbon very effectively [3]. By varying the H/D ratio, we can change the scattering length density from $0.9424 \cdot 10^{-6} \text{ \AA}^{-2}$ (pure C_7H_8) to $5.654 \cdot 10^{-6} \text{ \AA}^{-2}$ (pure C_7D_8), the latter being close to the value for (hexagonal) crystalline graphite ($7.5584 \cdot 10^{-6} \text{ \AA}^{-2}$). It should be noted that the real matrix density of our carbon ($\sim 1.85 \text{ g/cc}$) is lower than the calculated density of ideal hexagon graphite lattice because, in natural samples, as here, many types of defect are present, including, probably, closed pores.

Having obtained a liquid that closely matches the scattering density of the carbon matrix, this can be used to study the pore size distribution in the solid on the assumption that the pores will fill as a function of partial pressure according to the Kelvin Equation:

$$\ln \frac{p}{p_0} = -\frac{2\gamma V_m}{rRT} \quad (7)$$

Here p is the vapor pressure of the liquid in equilibrium with the sample and p_0 is its saturated vapor pressure, both taken at temperature T , γ is the surface tension of the liquid, V_m is its molar volume, r is the effective radius of the pore (excluding the thickness of the adsorbed surface layer, usually denoted as t) and R is the gas constant. Thus for liquids that wet the surface and for partial pressures lower than the saturated vapor pressure, p_0 , the liquid will have a concave curvature of radius r . Hence, all pores with radii less than r will be full of the liquid. If the liquid is contrast-matched, these pores will be invisible to SANS. Thus, we can separate the contribution to the scattering from pores of different radii.

5. Analysis of results

5.1 SANS data measured using variable contrast

The first series of SANS measurements were carried out using data collected with both the main and the high angle detectors on LOQ. The data were corrected for empty cell scattering and for background. It should be noted that there will be an additional flat background due to incoherent scattering that is proportional to the H content of the sample and toluene i.e. it increases with the H/D ratio. In order to find the best contrast-matching ratio, a series of samples were prepared with D-toluene contents of 0% (pure C_7H_8), 80%, 85%, 90% and 100% (pure C_7D_8). A double-logarithmic graph (Fig. 4) shows the scattering intensities as a function of Q for the different isotopic compositions where the reduction in intensity due to contrast matching is clear. The data for the dry sample show a linear region corresponding to a surface fractal at low Q , ($\sim Q^{-3.555}$) with a superimposed hump at high Q . Given that, for a surface fractal, we have that the scattering density varies as $Q^{-(6-D_s)}$, this corresponds to a surface fractal dimension of 2.445. At low Q , the intensity from the sample with fully deuterated toluene has a slope of -3.569 ($D_s = 2.431$), giving 1% reduction as compared with the dry sample. Recent SANS studies have compared a similar activated carbon with its carbonized precursor prior to activation [24] and the results clearly demonstrate that the

fractal component of the SANS corresponds to the carbon before activation while the hump is introduced by the activation process – a process that is in fact designed to produce nano-pores with 1-2 nm dimensions (Fig. 5). Comparison of the fractal dimensions before and after activation again gives very similar indices. The slope is -4 for the carbonized sample, i.e. very smooth surface, $d = 2$; and the slope for the activated sample is -3.58, i.e. a rough surface, $d = 2.42$ – surface fractal). The other main difference (seen over at least one order of magnitude in Q) is the substantial flat background prior to activation, presumably due to hydrogenous material removed during the activation process.

It should be noted that, after the background and incoherent scattering corrections, the scattering intensities from the evacuated sample and from the sample saturated with H-toluene have identical shapes, but with the latter having slightly higher intensity. As the scattering length density for H-toluene is small and positive, we would have

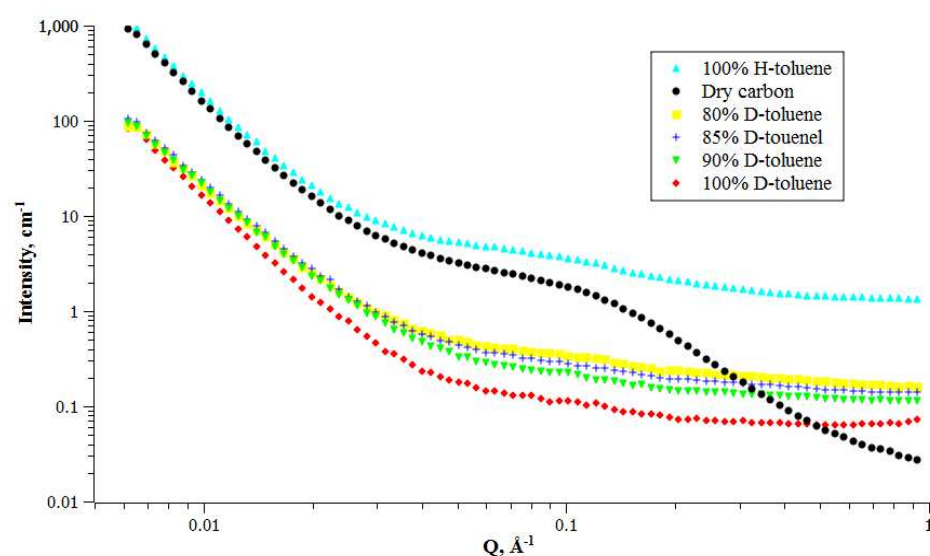


Fig 4. The SANS data from the activated carbon saturated with a series of liquids with different % of D-toluene content.

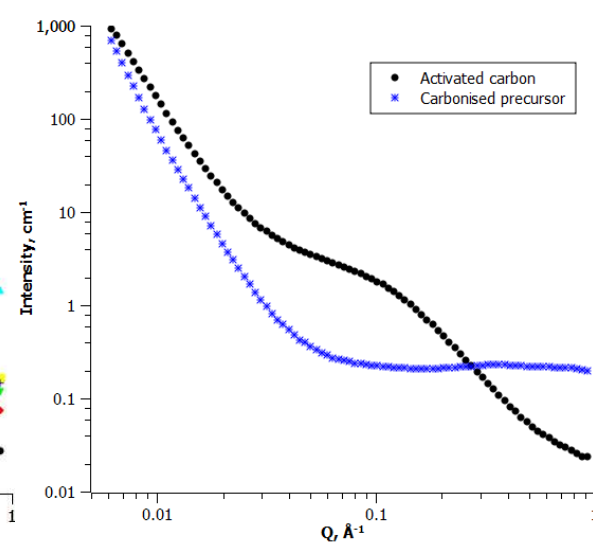


Fig. 5. The SANS data from activated carbon and carbonized precursor.

expected this sample to give a slightly lower intensity than the dry sample. One possible explanation for this small normalization error is that the addition of a liquid to the dry powder produces a slight densification of the sample within the beam area due to surface tension drawing the particles together. This effect is also seen in the second experiment described below which was performed using a different sample holder.

The variation of the measured SANS with the scattering density of the toluene, is shown in Fig. 6 at several Q values, where, as expected, a parabola gives a good fit to the data (Eq. 2). At low Q, the reduction in the scattering intensities for 100% D-toluene compared to 100% H-toluene is about one order of magnitude whereas, at high Q,

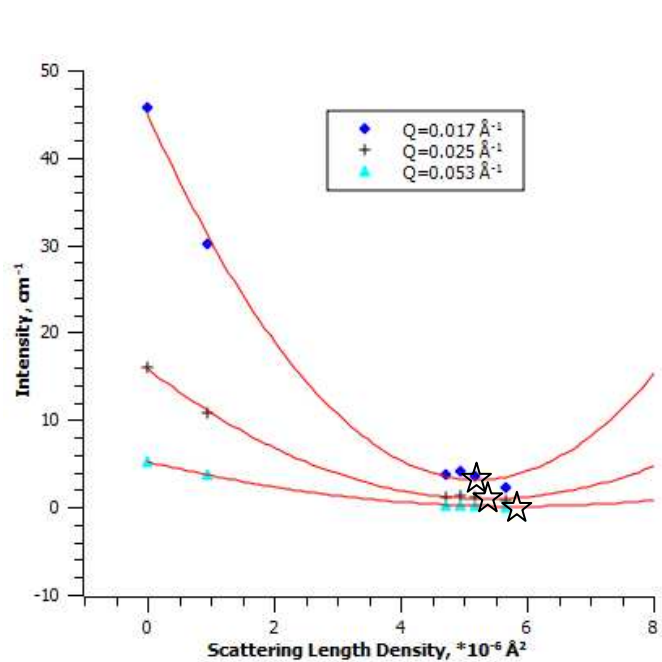


Fig. 6. Variation of the SANS signal with the scattering length density for H/D-toluene for a series of Q values. The star symbols show the fitted minimum scattering density at different Q values.

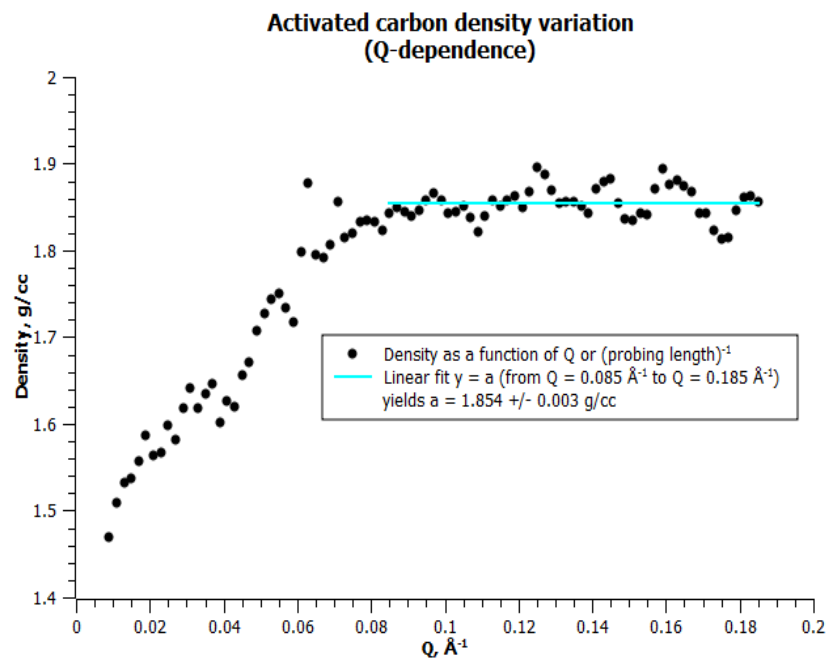


Fig. 7. Density variation with the wave vector transfer, Q.

this ratio is close to two orders of magnitude. It is clear that the match point is displaced to a rather higher scattering density at high Q. The Q-dependence of the contrast match point is shown in Fig. 7 where we have plotted the apparent carbon density from the match point against Q.

The origin of the apparent Q-dependence of the carbon density is clearly of interest and does not appear to have been noted by previous authors. It would seem very probable that the effect is due to the existence of closed porosity/defects or hydrogen-rich inclusions in the carbon matrix. Thus, if we compare the contrast over short distances ($1/Q$ small) across an accessible pore boundary, we will observe a region of full carbon density that, for graphite, should be about 2.15 g/cc. However, we found the density here approaching a maximum value of ~ 1.85 g/cc. If we increase our sampling distance (decreasing Q), the matrix density will be reduced as we are now averaging over increasing numbers of empty (inaccessible) pores and/or regions containing hydrogen. We thus conclude that the density of the carbon measured by contrast matching at different Q values can be thought of as

measuring the density from the surface using different “probing lengths”. It is notable (Fig. 8) that at high Q , (lengths less than 33\AA), there is a range of Q over which the apparent density varies as for a normal bulk solid ($d_m = 2.997$) whereas, for smaller Q values, $d_m = \sim 2.888$, which corresponds to a surface fractal behavior. It should also be noted that, at low Q , the fractal SANS scattering shows less effective contrast matching, suggesting that there are inaccessible pores/hydrogenous regions having the same fractal distribution that are not being contrast-matched, in agreement with the lower apparent density observed at these values of Q . However, it should also be noted that this effect could be in part due to changes in the toluene density in micropores.

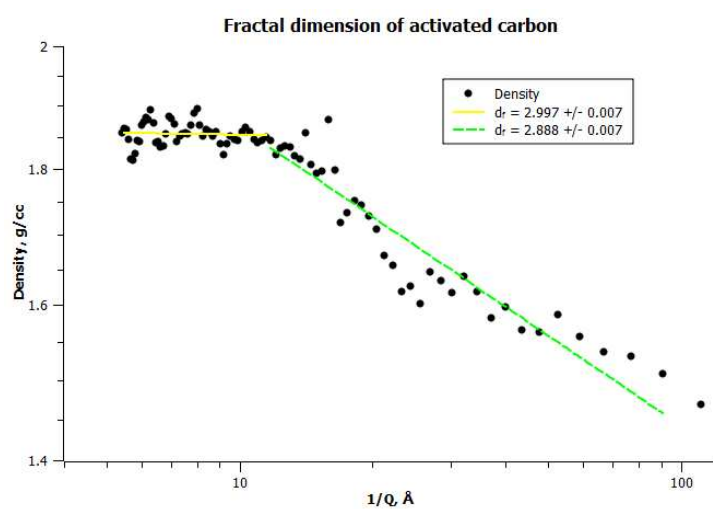


Fig. 8. Apparent Q -dependence of carbon density, derived from the scattering density of H/D-toluene at the contrast match point.

The discrepancies between values for the density of micro(nano)-porous activated carbon measured by helium pycnometry (2.035 g/cc) and by the neutron contrast matching technique can be attributed to excess adsorption of He in micro-pores (if we can neglect the effect of included hydrogen in the average scattering density of the carbon). It is known that helium density measurements in these materials performed at room temperature can be erroneous [25]. Indeed, GCMC calculations suggest [26]

that the average density of helium confined in sub-nanometer pores may exceed the bulk density by orders of magnitude due to gas interaction with the surface. This makes the pores look bigger than they actually are and hence the matrix density determined by He pycnometry comes out higher than it should be. This effect can be reduced by measuring the density at higher temperatures, but we found that on IGA an increase in temperature introduced an instability in the sample mass caused by convection. At 308K , the ratio between “He pore widths” and the geometrical pore widths in the range of $3\text{\AA} - 10\text{\AA}$ is predicted to be about $1.25 - 1.5$ [26]. Hence, the “He density” of the nano-pore carbon can be ca. 25% higher than densities derived from the neutron contrast matching method. This agrees well with the difference between experimental pycnometry and neutron scattering length density values for the present material. As liquid toluene is relatively incompressible (in small pores) compare to He

gas, the uncertainties in density determination by this method are considerably lower. Thus, for nanoporous material, the use of the SANS/Contrast matching technique should provide a more accurate density values than He picnometry.

5.2 SANS measured as a function of D-toluene partial pressure

In order to investigate the inner structure of the pores and their connectivity, the SANS signal was measured for the sample equilibrated with the matching liquid (D-toluene in our case) at a series of D-toluene partial pressures. By using D-toluene, we get as close as is possible to the situation where a pore filled with the condensed liquid ceases to be visible to the SANS. The filling and emptying of the pores should be governed by the Kelvin Equation, i.e. the curvature of the (surface-wetting) liquid is dictated by the partial pressure of the vapor. It is assumed that a pore will fill if the radius of curvature of its surface is less than the effective Kelvin radius of curvature of a surface meniscus at that partial pressure. Incidentally, it should be noted that the adsorption isotherms show no hysteresis for toluene absorption which implies that the pores are not linked to the surface of the carbon by apertures with significantly smaller dimensions than the dimensions of the toluene molecule, as seems reasonable for the activation process employed.

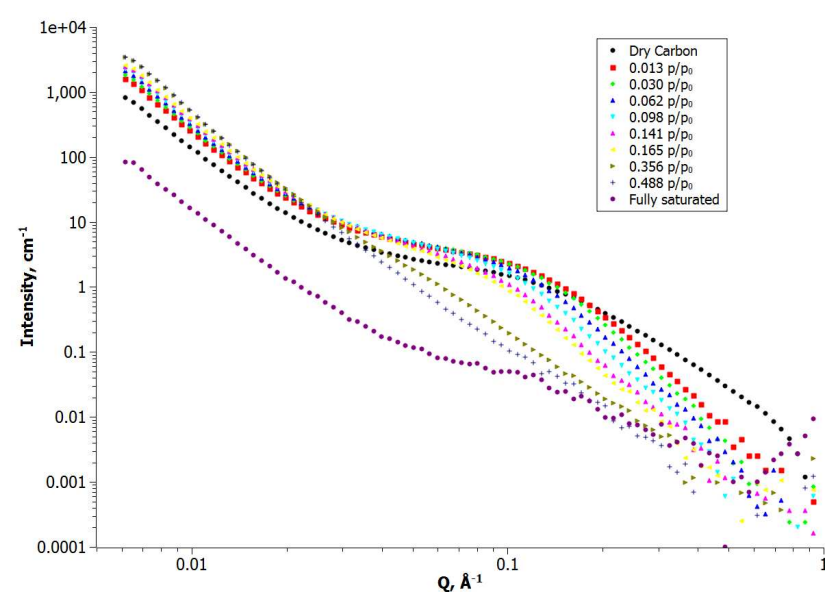


Fig. 9. SANS measurements from the activated carbon sample at a series of D-toluene partial pressures measured at 46 °C.

Following a measurement on the dry sample, D-toluene was added until the partial pressure reached $0.6 p/p_0$ – where p_0 is the saturated vapor pressure of D-toluene at the measurement temperature (46°C , $p_0 = 105 \text{ mbar}$) and the SANS was then measured. The partial pressure was then reduced in steps using a vacuum pump and, at each stage, the SANS was measured. The partial pressure was monitored using two Baratron

pressure gauges (full scales: 10 torr and 1000 mbar respectively) to provide a double check on the pressure. The 10 torr gauge was preferred over its calibrated pressure range.

Fig. 9 shows a log-log plot of the SANS data for the carbon at the measured D-toluene p/p_0 values during desorption at 46°C. At low Q , in the surface fractal region, as the partial pressure increases, the intensity first rises with increasing partial pressure to a maximum at about $p/p_0 = 0.5$ and then drops to the minimum value. At high Q , in contrast, the intensity drops continuously as p/p_0 increases and the micropores pores fill with the adsorbate.

It is interesting to analyze these measured intensities in terms of the “Porod Invariant” obtained by integration over the Q^2 -weighted SANS signal as a function of the D-toluene partial pressure to obtain the variation of the empty pore volume as a function of p/p_0 . The Porod Invariant (P.I.), is defined by:

$$P.I. = \int_0^{\infty} Q^2 \frac{d\Sigma}{d\Omega}(Q) dQ \quad (8)$$

From this expression, the empty pore volume in dry carbon can be extracted by applying the following relation [27],

$$P.I. = 2\pi^2 (\rho_c - \rho_p)^2 \varphi (1 - \varphi) \quad (9)$$

where φ is the fraction of the sample material that is occupied by empty pores and where ρ_c and ρ_p are the scattering length densities of carbon and empty pore respectively.

From (9), writing $P.I. / 2\pi^2 (\rho_c - \rho_p)^2 = F$, we should note that F is dimensionless and, if, as here, the SANS data is properly normalized, $0 < F < 0.25$ and hence

$$\varphi = 1/2 \pm \sqrt{1/4 - F} \quad (10)$$

Hence, we can extract two values for φ ($\varphi^+ + \varphi^- = 1$ as implied by the Babinet Principle). On this basis, assuming the perfect normalization of the data, the total pore fraction for the dry sample, φ_0 , is found to be 0.294, giving a

Partial pressure of D-toluene at 46°C	Fraction pores filled by D-toluene
0.0	0.0
0.013	0.416
0.030	0.527
0.062	0.635
0.098	0.742
0.141	0.816
0.165	0.847
0.356	0.921
0.488	0.946
1.0	1.0

Table 1. Values for the partial pressure values of D-toluene at 46°C and the corresponding values for the fraction of empty pores at that p/p_0 value as extracted from the SANS data using the Porod Invariant.

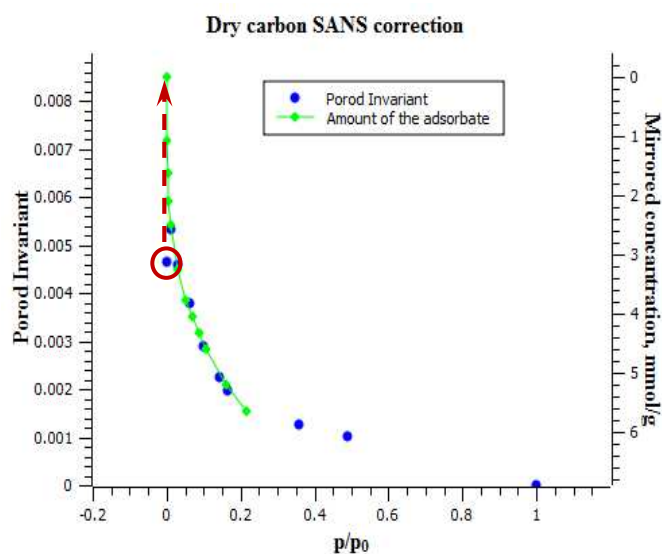


Fig. 10. Dry sample Porod Invariant correction.

bulk density of 1.3 g/cc. This value falls within 11% of the bulk density of 1.46 g/cc as obtained using contrast matching for the smallest wave vector (0.00618\AA^{-1}). The corresponding $[\varphi(p/p_0)/\varphi_0]$ values have been extracted at each pressure step and the resulting values are presented in the Table 1. The fraction of pores filled by D-toluene is thus given by $1 - [\varphi(p/p_0)/\varphi_0]$. This measurement yields a smaller value of the fractional pore volume than either the vapour adsorption measurements – which omit the largest radius pores – and the mercury penetrometry values – which omit the smaller pores. However, it should be noted that the actual porosity obtained from the Porod Invariant must in fact be smaller than the full porosity because of the low Q limit used in the determination of the P. I., which therefore only includes the porosity smaller than $\approx 10\text{nm}$.

The Porod Invariant is a useful tool both for the elucidation of porosity evolution as a function of partial pressure of the contrast matching liquid and also for checking the inter-normalization of separate runs. The scattering intensities from the dry carbon in both contrast match and partial pressure variation experiments were noted to have been reduced in comparison with the wetted carbon samples. The

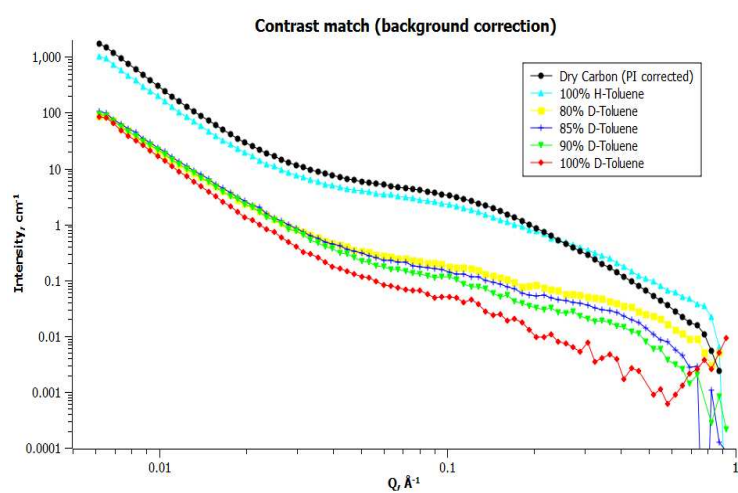


Fig. 11. Contrast matching SANS data with corrected intensities for a dry sample.

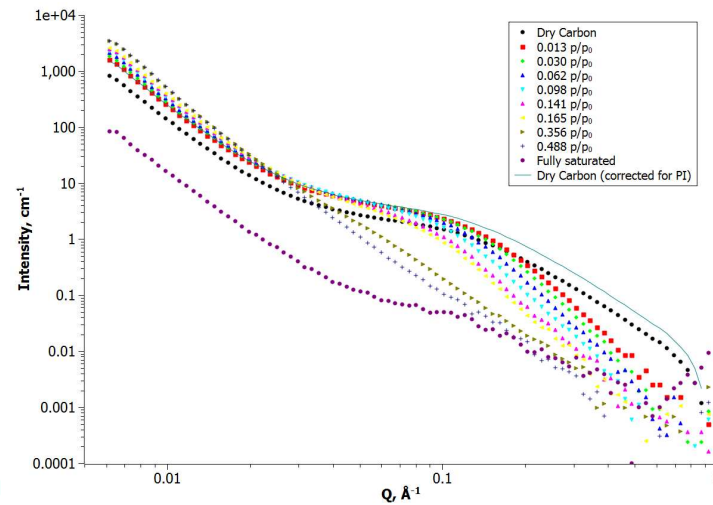


Fig. 12. Partial pressure variation SANS data (subtracted background) corrected for a dry sample.

presumed reason for this is that there is a densification effect caused by the surface tension of toluene: when toluene is added to the sample, as suggested above, it drags the carbon powder particles closer together, bringing more sample mass into the beam area. The SANS measured on dry carbon should thus be corrected for this effect in order to present a comparative set of data. This could be done when the Porod Invariant is compared with the gravimetric data on toluene sorption (Fig. 10). The value of the Porod Invariant at zero pressure (circled in red) can be corrected in accordance with concentration zero-point position (RHS) relatively to the Porod Invariant scale (LHS). The initial value of the P.I. at $p/p_0 = 0$ is corrected to be 0.0086 with a scaling coefficient of 1.85. Thus, the scattering intensities multiplied by this factor correspond to the corrected SANS data (Fig. 11, 12).

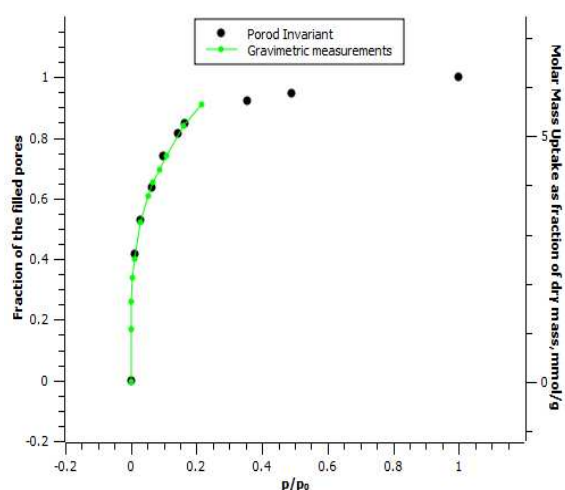


Fig. 13. Plot of fraction of filled pores ϕ , extracted from (a) the Porod Invariant (LHS scale) and (b) the gravimetric isotherm as a function of p/p_0 % (RHS Scale) internormalized by equating 100% pore filling to 6.25 mmol/g of toluene.

It is of interest to compare these data from Table I with the measured D-toluene uptake isotherm as measured gravimetrically. The agreement between the mass uptake curve and the calculated fraction of filled pores is remarkable (Fig. 13).

5.3 Model for fitting the Pore Size Distribution

In order to fit the full SANS signal, it is necessary to introduce a model that adds a fractal term to a function describing the scattering from a poly-disperse distribution of micropores. There are many model scattering functions available in the literature that can be incorporated in general fitting programs such as FISH⁷. However, to extract physically meaningful parameters, the number of parameters used must be kept to a minimum while describing a physically reasonable model for the scattering. In the present case, it is reasonable to describe the high Q hump due to the micro-pores by a Guinier Function for $F(Q)$ with a suitable distribution of pore radii, $P(r)$, and to assume that $S(Q)$ is a constant as for a random distribution of such pores. For modeling $P(r)$, we have used an exponentially decaying function for the distribution of pore volumes, $V(r)$, above a cut-off radius of r_p , appropriate to a particular partial pressure. This yields a model for the scattering from the micropores of the form:

$$\langle |F(Q)|^2 \rangle_p = \int_{r_p}^{\infty} e^{-\gamma r} e^{-\frac{Q^2 r^2}{5}} dr \quad (11)$$

Note that, in terms of the pore radius distribution, $P(r)$, this integral would be written:

$$\langle |F(Q)|^2 \rangle = \int_{r_p}^{\infty} \frac{4\pi r^3}{3} P(r) e^{-\frac{Q^2 r^2}{5}} dr, \quad (12)$$

where $P(r) = \frac{3}{4\pi r^3} e^{-\gamma r}$

Integration [28] over r for $r_p < r < \infty$ yields the following expression for $\langle |F(Q)|^2 \rangle_p$:

$$\frac{\sqrt{5\pi} e^{\frac{5\gamma^2}{4Q^2}} \left(1 - \operatorname{erf} \left(\frac{5\gamma + 2Q^2 r_p}{2\sqrt{5}Q} \right) \right)}{2Q} \quad (13)$$

⁷ <http://www.small-angle.ac.uk/small-angle/Software/FISH.html>

Writing the full expression for the cross section we now have:

$$\frac{d\Sigma}{d\Omega}(Q) = A_p Q^{-(6-D_{sp})} + c_p \langle |F(Q)|^2 \rangle_p + B_{inc.p} \quad (14)$$

The first term in Eq. 14 describes the scattering from a fractal, the second term corresponds to the signal from micropores – appearing as a “hump” in the middle Q range, and the last term is an incoherent background, all attributed to a specific partial pressure.

The first term in Eq. 14 describes the scattering from a fractal, the second term corresponds to the signal from micropores – appearing as a “hump” in the middle Q range, and the last term is an incoherent background, all attributed to a specific partial pressure. The resulting curves fitted to the SANS data for all values of p/p_0 , using r_p , A_p , D_{sp} , c_p , $B_{inc.p}$ and γ as fitting parameters show good agreement with the experimental data. The values of the fitted parameters are shown in Table 2. Two examples of the fitted data are demonstrated in Fig. 14. They show

Pressure, mbar	Pore radius, r_p , Å	Scaling coefficient, c_p	γ_p	$A_p, *e^{-6}$	D_{sp}
0	9.2	0.5722	0.0578	9.452	2.281
1.35	12.0	0.6005	0.0548	4.162	2.111
3.15	13.1	0.5557	0.0434	3.571	2.053
6.55	14.4	0.4761	0.0446	3.444	2.016
10.4	15.6	0.4975	0.0415	3.601	2.005
15.0	17.7	0.4601	0.0402	5.117	2.059
17.5	18.7	0.4580	0.0384	4.949	2.045
37.8	29.0	0.5850	0.0569	4.852	2.040
51.8	33.4	0.5826	0.0595	4.558	2.004

Table 2. Parameters fitted to the measured SANS cross sections as a function of p/p_0 .

small deviations between experimental and fitted curves in the middle of the Q range around the activation “hump” – presumably because the exponential form we adopted is not perfect. However, as p/p_0 increases, these discrepancies become less noticeable. The measured scattering also shows a tail at high Q that corresponds to very small pores. It is notable that this contribution seems to be independent of p/p_0 . This suggests that it may originate from small pores that are inaccessible to the D-toluene – either because they are too small to accommodate these

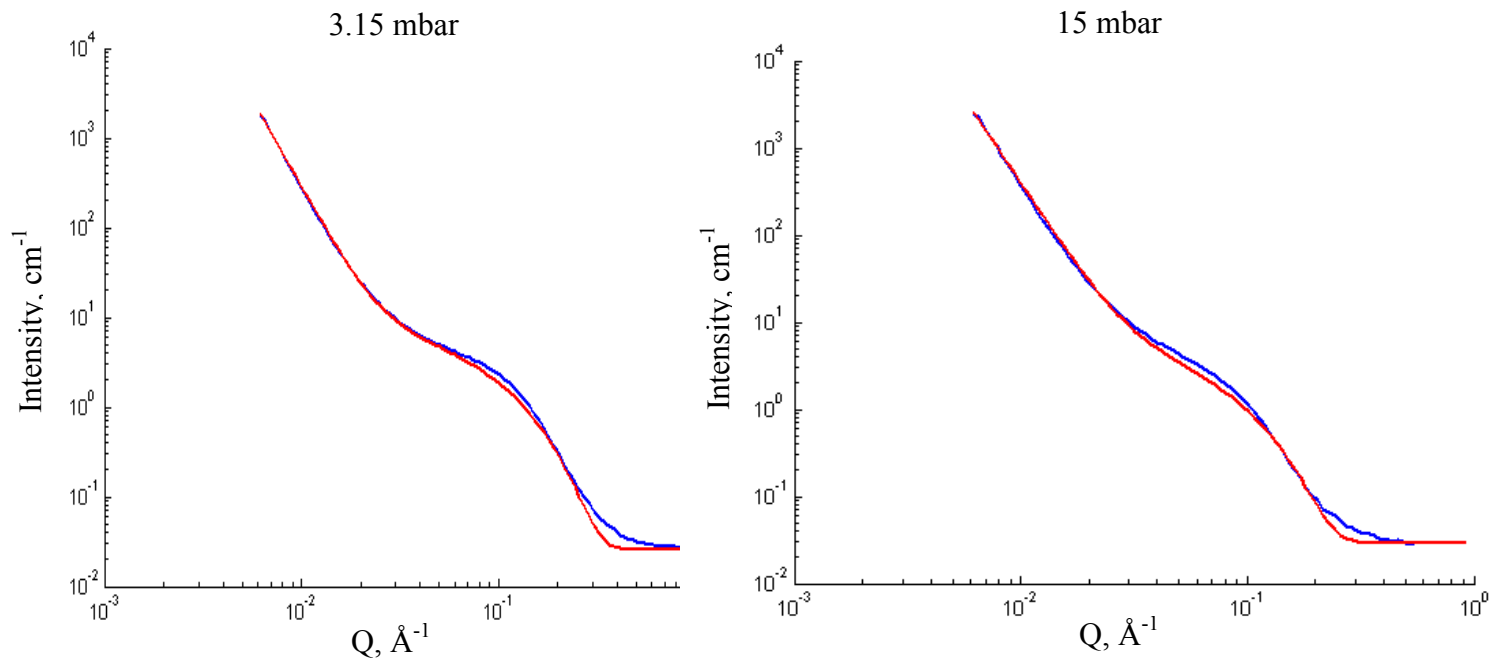


Fig. 14. Fitting curves (red) to the experimental SANS data (blue) for two specific partial pressures.

molecules or because they are internal. This is not unexpected, given the difference between the measured skeletal density of the activated carbon (1.85 g/cc) and the theoretical density of graphite.

It is of interest to plot values of $\ln(p/p_0)$ versus the inverse of the fitted pore radius at pressure p , r_p , and hence, to employ the Kelvin equation to estimate the surface tension of D-toluene [29]. The data are plotted in Fig. 15 and show two distinct gradients. Strictly speaking, the Kelvin equation is only applicable to the larger radius pores. The lower limit of validity could be taken as the point where the meniscus disappears. Bering et al. [30] noted that in some cases the Kelvin equation is only valid down to a radius of 15-16Å. If we assume that it is actually valid for pore radii larger than 29Å, the slope gives very precisely the surface tension of D-toluene (25.4 mN/m). As the pores become smaller, the experimental data diverge from the Kelvin equation. One possible reason for this could be a change in the apparent surface tension of the liquid when confined in very small pores. The average linear fit

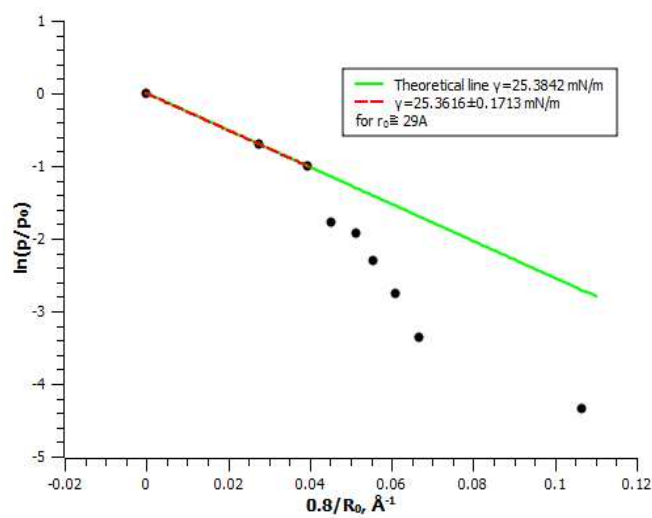


Fig. 15. Validity of Kelvin equation for pore radii ≥ 29 Å.

for all radii shows a surface tension of 41.1756 mN/m, about double the macroscopic value. Broseta et al. [31] performed similar SANS wetting experiments using water. By applying the Kelvin equation to their experimental data they found a surface tension for water of around twice its macroscopic value. This is consistent with our value for the deviation of the toluene surface tension from its bulk value when averaged over all pore radii.

6. Conclusion

The power of the SANS/contrast matching method has been demonstrated for an activated carbon using H/D toluene. It is shown that the apparent density of carbon at the match point is Q-dependent, with a constant density at high Q that is close to the skeletal density of the carbon. The best possible contrast match is actually produced with 100% D-toluene. At lower Q, the apparent density gets smaller, as presumably the measuring range increases and inaccessible pores are included in the averaged density. The SANS signal for the dry carbon shows a hump at higher Q which is superimposed on a fractal form that dominates at low Q. A comparison with a measurement on the same material prior to the activation process confirms that this hump is produced by the activation process. This process also removes a flat incoherent signal due to hydrogen in the sample and somewhat changes the fractal power law. The SANS was then measured as a function of the partial pressure (p/p_0) of D-toluene. As the partial pressure is increased from zero, the smallest pores fill first. These data are analyzed in terms of the Porod Invariant yielding a curve for the total porosity as a function of partial pressure. This agrees well with the liquid adsorption isotherm as measured gravimetrically. The Porod Invariant porosities, when compared with gravimetric toluene vapor absorption data, were used to correct the dry carbon SANS intensities for the densification effect. The SANS has been fitted using a function that represents the fractal component in the scattering with an additional term representing the hump in the pore size distribution assuming that the SANS can be represented using a polydisperse

version of the Guinier Distribution with a cut-off radius determined by the partial pressure. This allows us to determine the small radius limit to the pore-size distribution as a function of p/p_0 . Now, according to the Kelvin equation, if we plot $\ln(p/p_0)$ versus $1/r$, the gradient (for the larger radii) yields a good value for the surface tension of toluene. The value obtained for larger pore radii agrees well with the bulk value for D-toluene. If we average over the full ($1/r$) range, the value obtained is about twice as large, which agrees with previously observed behavior.

Acknowledgements

One of us (MZ) would like to acknowledge the provision of a studentship by the University of Salford. DW would also like to acknowledge support from AWE. We would also like to acknowledge the STFC and ISIS for the provision of neutron beam time on LOQ (Experiment RB920460).

References

- [1] Ross DK. Hydrogen storage: The major technological barrier to the development of hydrogen fuel cell cars. *Vacuum* 2006; 80: 1084-1089
- [2] McNicholas TP, Wang AM, O'Neill K, Anderson RJ, Stadie, NP, Kleinhammes A, et al. H₂ storage in microporous carbons from PEEK precursors. *J. Phys. Chem. C* 2010; 114: 13902-13908.
- [3] Calo JM, Hall PJ. The application of small angle scattering techniques to porosity characterization in carbons. *Carbon* 2004; 42: 1299-1304.
- [4] Li JC, Ross DK, Howe LD, Stefanopoulos KL, Fairclough, JPA, Heenan R, Ibel K. Small angle neutron scattering studies of the fractal-like network formed during desorption and adsorption of water in porous materials. *Phys. Rev. B* 1994; 49:5911-5917i
- [5] Bale HD, Schmidt PW. Small-angle X-ray scattering investigation of sub-microscopic porosity with fractal properties. *Phys. Rev. Lett.* 1984; 53: 596 - 599.

- [6] Diduszko R, Swiatkowski A, Trznadel BJ. On surface of micropores and fractal dimension of activated carbon determined on the basis of adsorption and SAXS investigations. *Carbon* 2000; 38:1153-1162.
- [7] He LL, Chathoth SM, Melnichenko YB, Presser V, McDonough J, Goyotsi Y. Small-angle neutron scattering characterization of the structure of nanoporous carbons for energy-related applications. *Microporous and Mesoporous Materials* 2012 ; 149 46-54.
- [8] Mergia K, Stefanopoulos KL, Ordas N, Garcia-Rosales C. A comparative study of the porosity of doped graphites by small angle neutron scattering, nitrogen adsorption and helium pycnometry. *Microporous and Mesoporous Materials* 2010; 134:141-149.
- [9] Mascotto S, Wallacher D, Brandt A, Hauss T, Thommes M, Zichler GA, et al. Analysis of microporosity in ordered mesoporous hierarchically structured silica by combining physisorption with *in situ* small-angle scattering (SAXS and SANS). *Langmuir* 2009; 25:12670-12681.
- [10] Benham MJ, Ross DK. Experimental determination of absorption-desorption isotherms by computer-controlled gravimetric analysis. *Z. Physik. Chemie NF* 1989;163:S25-32.
- [11] Broekhoff JCP, de Boer JH. Studies of pore systems in catalysts: XII Pore distributions from the desorption branch of a nitrogen sorption isotherm in the case of cylindrical pores. A. An analysis of the capillary evaporation process. *J. Catalysis* 1968; 10:368-376.
- [12] Halsey G, Physical adsorption on non-uniform surfaces. *J. Chem. Phys.* 1948; 16:931.
- [13] Dubinin MM, Astakhov VA. Description of adsorption equilibria of vapours on zeolites over wide ranges of temperature and pressure. *Adv. Chem. Series* 1971; 102:69-&.
- [14] Heenan RK, King SM, Osborn R, Stanley HB. COLETTE Users Guide. Rutherford Appleton Laboratory Report, RAL-89-128, 1989; King SM, Heenan RK. Using COLETTE. Rutherford Appleton Laboratory Report, RAL-95-005, 1995.
- [15] Wignall GD, Bates FS. Absolute calibration of small-angle neutron scattering data. *J. Appl. Crystallogr.* 1987; 20: 28.

- [16] King SM. In: Pethrick RA, Dawkins JV, editors. Modern techniques for polymer characterisation, New York: John Wiley, 1999; p171.
- [17] Pfeifer P, Obert M. In Avnir D, editor. The Fractal Approach to Heterogeneous Chemistry, New York: Wiley; 1989; p. 11.
- [18] Pfeifer P, Ehrburger-Dolle F, Rieker TP, Gonzalez MT, Hoffman WP, Molina-Sabio M, et al. Nearly space-filling fractal networks of carbon nanopores. Phys. Rev. Lettrs. 2002; 88:115502.
- [19] Bunde A, Halvin S. Fractals and Disordered Systems. Berlin: Springer-Verlag; 1991, p. 229.
- [20] Mandelbrot BB. The Fractal Geometry of Nature. New York: W.H. Freeman and Company; 1982.
- [21] Winter R, Gabke A, Czeslik C, Pfeifer P. Power-law fluctuations in phase-separated lipid membranes. Phys. Rev. E 1999; 60:7354-7359.
- [22] Freltoft T, Kjems JK, Sinha SK. Power law correlations and finite size effects in silica particle aggregates studied by small-angle neutron scattering. Phys. Rev. B 1986; **33**: 269 – 275.
- [23] Porod G. General Theory. In: Glatter O, Kratky O, Editors. Small Angle X-Ray Scattering, London: Academic Press, 1982, p 17-52.
- [24] Mileeva Z and Ross DK. The effect of the activation process on an activated carbon studied by Small Angle Neutron Scattering. Macroporous and Mesoporous Materials, to be published.
- [25] Malbrunot P, Vidal D, Vermesse J, Chahine R Bose TK. Adsorbent helium density measurement and its effect on adsorption isotherms at high pressure. Langmuir 1997; 13: 539-544.
- [26] Neimark NV and Ravikovitch PI. Calibration of pore volume in adsorption experiments and theoretical models. Langmuir 1997; **13**: 5148-5160.
- [27] Higgins JS, Benoit HC. Polymers and Neutron Scattering: Oxford Series on Neutron Scattering in Condensed Matter, 8, Oxford: Oxford University Press, 1997.
- [28] Jeffrey A, Zwillinger D. Tables of Integrals, Series, and Products, New York: Academic Press, 7th Edition; 2007.

- [29] Gaines GL, Legrand DG. The surface tension of some deuterated hydrocarbons. *Colloids and Surfaces A: Physicochemical and Engineering Aspects* 1994; 82 : 299-300.
- [30] Bering BP, Dubinin MM, Serpinsky VV. Adsorption of argon and nitrogen on NaX zeolite modified by treatment with water. *J. Colloid. Interface Sci.* 1966; 21: 378
- [31] Broseta D, Barre L, Viziki O, Shahidzadeh N, Guilbaud JP, Lyonard S. Capillary condensation in a fractal porous medium. *Phys. Rev. Lettrs.* 2001; 86:5313 – 5316.

Tables.

Table 1. Values for the partial pressure values of D-toluene at 46°C and the corresponding values for the fraction of empty pores at that p/p_0 value as extracted from the SANS data using the Porod Invariant.

Table 2. Parameters fitted to the measured SANS cross sections as a function of p/p_0 .

Figures.

Fig. 1. Pore size distribution according to De-Boer and Halsey models from nitrogen sorption. Inset: Nitrogen sorption isotherm at 80K.

Fig. 2. Pore size distribution according to De-Boer and Halsey models from toluene sorption. Inset: Toluene sorption isotherm at RT.

Fig. 3. Exploded view of the cell and sample holder used for the variable partial pressure experiments and their position in the neutron beam line.

Fig. 4. The SANS data from the activated carbon saturated with a series of liquids with different % of D-toluene content.

Fig. 5. The SANS scattering from activated carbon and carbonised precursor.

Fig. 6. Variation of the SANS signal with the scattering length density for H/D-toluene for a series of Q values. The star symbols show the fitted minimum scattering position.

Fig. 7. Density variation with the wave vector transfer, Q.

Fig. 8. Apparent Q-dependence of carbon density, derived from the scattering density of H/D-toluene at the contrast match point.

Fig. 9. SANS measurements from the activated carbon sample at a series of D-toluene partial pressures measured at 46 °C.

Fig. 10. Dry sample Porod Invariant correction.

Fig. 11. Contrast matching SANS data with corrected intensities for a dry sample.

Fig. 12. Partial pressure variation SANS data (subtracted background) corrected for a dry sample.

Fig. 13. Plot of fraction of filled pores, extracted from (a) the Porod Invariant (LHS scale) and (b) the gravimetric isotherm as a function of p/p_0 (RHS Scale) internormalised by equating 100% pore filling to 6.25 mmol/g.

Fig. 14. Fitting curves (red) to the experimental SANS data (blue).

Fig. 15. Validity of Kelvin Equation for pore radii ≥ 29 Å.